Dalton Transactions

Accepted Manuscript

ROYAL SOCIETY OF CHEMISTRY

www.rsc.org/dalton

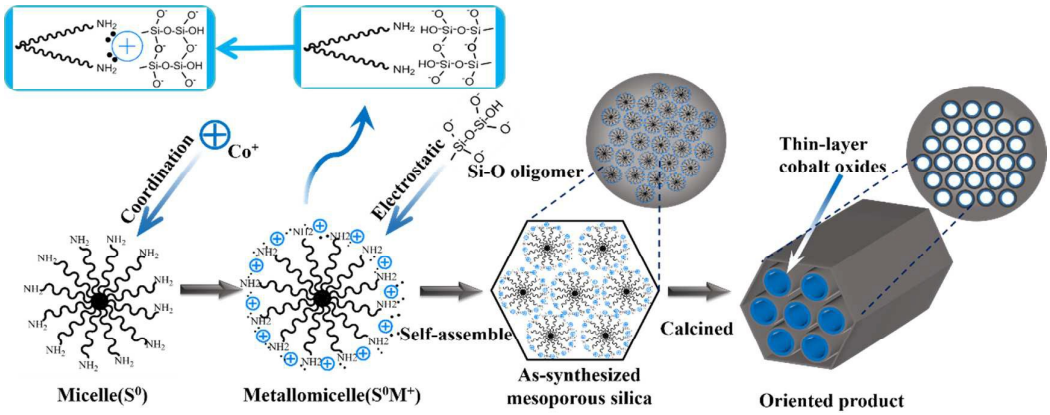

Scheme. 1 Metal-assisted templating route ($S^0X^+I^-$) for synthesis of nanospherical HMS-Co

Nanospherical hexagonal mesoporous silica (HMS) with functional mesochannel covered with thin-layer-dispersed cobalt oxide species was directly fabricated via a novel metal-assisted templating method ($S^0M^+I^-$). In this special method, cobalt ions would be enriched on the surface of pore wall by the physicochemical interaction among the surfactant, cobalt ions and silicate oligomers. Typically, a metallomicelle template (S^0M^+) formed from the coordinative assembly of metal cation (Co^{2+}, M^+) with neutral surfactant dodecyl amine (DDA, S^0) would match with negatively charged silicate oligomers (I^-) by electrostatic interaction to assemble into the Co-modified HMS nanosphere.

Metal-assisted templating route ($S^0M^+I^-$) for fabricating thin-layer CoO covered on the channel of nanospherical-HMS with improved catalytic properties

Fu Yang, Shijian Zhou, Haiqing Wang, Saifu Long, Xianfeng Liu, Yan Kong*

State Key Laboratory of Materials-Oriented Chemical Engineering, College of Chemistry and Chemical Engineering, Nanjing Tech University, Nanjing 210009, Jiangsu, P. R. China

*Corresponding author, E-mail: kongy36@njtech.edu.cn (Y, Kong), Tel: (86)-25-83587860.

Abstract: Nanospherical hexagonal mesoporous silica (HMS) with functional mesochannel covered with thin-layer-dispersed cobalt oxide species was directly fabricated via a novel metal-assisted templating method ($S^0M^+I^-$). In this special method, cobalt ions would be enriched on the surface of pore wall by the physicochemical interaction among the surfactant, cobalt ions and silica. Typically, a metallomicelle template (S^0M^+) formed from the coordinative assembly of metal cation (Co^{2+}, M^+) with neutral surfactant dodecyl amine (DDA, S^0) would match with negatively charged silicate oligomers (I^-) by countra-ion interaction to assemble into the Co-modified HMS nanosphere. The metallization of DDA micelles and the role of cobalt ions in the assemble process can be demonstrated. Interestingly, the adding amounts of cobalt apparently affect the size of the HMS nanosphere. Additionally, the coverage of CoO species on the mesochannel is increased with cobalt ions coordinated on the micelles. Finally, the functional Co-HMS with dispersed catalytic active phase and improved structure exhibits a special catalytic activity (yield of ca. 65%) for direct oxidation of phenol to b-benzoquinone by the assistance of sulfate radical stimulated from cobalt in the presence of peroxymonosulfate.

Keywords: Metallomicelles, Thin-layer-dispersed, Cobalt oxide, Nanosphere, b-benzoquinone.

1. Introduction

Supported cobalt-based catalysts have exhibited many potential applications in heterogeneous catalytic reaction fields such as the oxidation of benzene[1, 2] and styrene,[3] Fischer-Tropsch synthesis,[4] etc. Recently, some investigations have reported that sulfate radicals, generated from peroxymonosulfate (PMS) in the presence of a cobalt-based catalyst, can effectively oxidize phenolic compounds and lead to their fast degradation.[5-9] This type of Co^{2+}/PMS system is regarded like a modified Fenton reaction (Fe^{2+}/H_2O_2). Additionally, due to higher oxidation potential of sulfate radical [2.5–3.1 eV] as compared to hydroxyl radical [2.7 eV], much faster reaction rate for oxidation can be achieved in sulfate radical process than in Fenton oxidation.[7] Therefore, the investigation on cobalt-based catalyst in Fenton-type reactions especially for obtaining highly-efficient and stable supported catalyst is highly significant.

Mesoporous silica, as special carrier or reactor, has been widely researched on the nano-/microscale due to its large surface area, oriented-ordered channel and appropriate pore volume.[10-12] However, the poor hydrothermal stability of mesoporous silica leads to its more adaptability in some relatively mild reactions just like Fenton-like reaction. With regard to its catalysis applications, the status of active sites,[13, 14] structural properties and morphology of support[15, 16] especially play important roles in determining the catalytic performance of mesoporous silica. Generally, the catalysts with highly-dispersed and accessible catalytic active sites or special morphology and superior structural properties tend to contribute significantly to high catalytic activity.[17-22] Typically, nanospherical catalyst, such as transition metal modified spherical MCM-41[23, 24]/48,[25] have been reported for their excellent catalytic activities. However, the numbers of active sites on the intra-pore surface of the metal-doping mesoporous silica were still insufficient. A large number of active metal atoms may be deeply incorporated

in the inner-framework of mesoporous silica. Therefore, it is highly-desirable to obtain surface-functional mesopore with mono-layer dispersed transition metal oxides phase, especially for spherical mesoporous silica.

In addition, so far, the cation (S^+I^-),[26] anion ($S^-X^+I^-$),[27] and neutral (S^0I^0)[28] templating pathways have been applied to prepare mesoporous silica such as MCM, AMS and HMS. MCM series synthesized with cation (S^+I^-) templating route afford long-range hexagonal structures, while HMS series prepared by neutral (S^0I^0) templating route are based on hydrogen bonding and self-assembly between neutral primary amine surfactants (S^0) and neutral inorganic precursors (I^0). Owing to the weaker assembly forces, the textural properties of HMS are inferior to that of the MCM series,[29] Therefore, the HMS material assembled just by hydrogen bonding interaction would not be on a par with MCM series materials assembled with counterion-mediated interaction.

Herein, on the basis of above thoughts, we proposed a novel metal-assisted templating route ($S^0M^+I^-$) to prepare cobalt-based mesoporous silica HMS materials possessing thin-layer-dispersed catalytic active phase and improved mesoporous structure. In this method, the metallomicelles (S^0M^+) from coordinated-assembly of cations of Co^{2+} and neutral surfactant (DDA) were used as cationic-like template to directly prepare the mesoporous silica with Co-modified mesoporous wall. Various efficient characterization techniques were utilized to demonstrate the structure of the mesocomposites, state of CoO species and the involved template method. Finally, a Fenton-like model reaction for oxidation of phenol in the presence of peroxymononsulfate was used to evaluate the catalytic activities of the obtained nanospherical HMS-Co material.

2. Experimental Section

2.1 Chemicals and Materials

Dodecyl amine (DDA, ≥98%) was purchased from Aladdin. Cobalt chloride hexahydrate ($CoCl_2 \cdot 6H_2O$, ≥99%), tetraethylorthosilicate (TEOS, AR) and phenol (≥99%) were purchased from Sinopharm Chemical Reagent Co., Ltd. Oxone (peroxymononsulfate, PMS, $2KHSO_5 \cdot KHSO_4 \cdot K_2SO_4$) was obtained from Aldrich. All chemicals were commercially available and were used as received.

2.2 Synthesis of nanospherical Co-HMS

The typical prepared process for the metal-assisted assembly of the mesocomposites is as follows: 1.85 g DDA (0.01 mol) was dissolved in a mixed solution containing 62.5 ml deionized water and 18 ml ethanol and stirred for 30 min in 45 °C water bath. The addition of different amounts of $CoCl_2 \cdot 6H_2O$ (1, 2, 3 and 4 mmol) led to the color of solutions turning from pink to dark green immediately, which could be referenced from Fig. S1. After cooled to room temperature, 10.73 ml of TEOS was subsequently added with vigorous stirring for another 4 h and then kept static for 18 h in 45 °C water bath. Finally, the resulting samples were centrifuged and washed for three times with ethanol and water. The as-synthesized samples were annealed at 550 °C for 6 h in dry air steam. The samples corresponding to different cobalt amount were designated as HMS-xCo (x= 1, 2, 3, 4).

2.3 Synthesis of Co-doping HMS

For purposes of comparison, Co-doping HMS was prepared by co-condensation method according to the previous reported literature.[30] Typical prepared procedure was as follow: 1.85 g of DDA was dissolved in 25 mL of ethanol solution, then 62.5 mL of deionized water was added under vigorous stirring in 45 °C water bath. Subsequently, the certain amount of TEOS/$Co(NH_3)_4^{2+}$ (with molar ratio is 1.6) in ammonia and

ethanol solution was added dropwise to above solution, and the resulting solution was retained vigorous stirring for 4 h and kept static conditions at 45 °C for another 18 h. Finally, the obtained solid was isolated on a filter and washed, followed by calcination at 550 °C for 5 h in air. The obtained sample was designated as HMS-3Co (d).

2.4 Synthesis of post-impregnated Co-modified HMS

Cobalt-supported HMS was also prepared by the wetness impregnation method. As-made bare HMS was treated with the appropriate amounts of an ethanol solution of $CoCl_2 \cdot 6H_2O$ and the ethanol was rota-evaporated until complete dryness. After drying at 100 °C for 2 h, the final product was calcined at 550 °C for 5 h in air. The obtained sample was designated as HMS-3Co (p).

2.5 Characterization

The XRD patterns of the samples were collected with Smartlab TM 9 KW (Rigaku Corporation, Tokyo, Japan) equipped with a rotating anode and Cu Kα radiation (λ = 0.154178 nm).

The N_2 (77.4 K) adsorption-desorption measurements were carried out with BELSORP-MINI volumetric adsorption analyzer (BEL Japan, Osaka, Japan) in a relative pressure range P/P_0 from 0.01 to 0.99. The annealed samples were outgassed in vacuum at 150 °C for 5 h and before measurements. The specific surface areas and distribution of pore size were calculated using the Brunauer-Emmet-Teller (BET) and Barrett-Joyner-Halenda (BJH) methods, respectively.

Field emission scanning electron microscopy (FE-SEM) was performed on a Hitachi S4800 Field Emission Scanning Electron Microscopy (Hitachi, Tokyo, Japan).

High-resolution transmission electron microscopy (HRTEM) and scanning transmission electron microscopy (STEM) images were recorded on a JEM-2010 EX microscope

(JEOL, Tokyo, Japan), which was operated at an accelerating voltage of 200 kV. The samples were crushed in A.R. grade ethanol and the resulting suspension was allowed to dry on carbon film supported on copper grids.

Fourier Transform Infrared (FT-IR) spectra from the samples were obtained in the range of 400-4000 cm^{-1}, with powders dispersed on the KBr on Bruker VECTOR22 resolution (Bruker, Bruker, Germany).

Diffused Reflection UV-Vis spectra of samples were obtained in the range of 200-800 nm by Lambda 950 spectrophotometer (PerkinElmer, Waltham, MA, USA).

The X-ray photoelectron spectra (XPS) were performed on a PHI 5000 Versa Probe X-ray photoelectron spectrometer (ULVAC-PHI, Kanagawa, Japan) equipped with Al K_α radiation (1486.6 eV). The C1s peak at 284.6 eV was used as the reference for binding energies.

The cobalt content in the samples were determined using a PE Optima 2000DV (PerkinElmer, Waltham, MA, USA) Inductively Coupling Plasma emission spectrometer (ICP). The samples were completely dissolved in hydrofluoric acid before analysis.

The UV-visible absorption spectra of the micelles were analyzed by a UV-Vis spectrophotometer (BLV-GHX-V, Bilang Corporation, Shanghai, china).

2.6 Catalysis assess

The catalytic performance of the prepared samples was evaluated by the catalytic oxidation of phenol with the assistance of oxone. The reaction was carried out in a 100 mL reactor containing 30 ppm of phenol solution at room temperature. The reaction mixture was stirred constantly to maintain a homogeneous solution. A certain amount of oxidant, oxone, at a concentration of 6 mmol L^{-1}, was added to the mixture and allowed to dissolve before the reaction. Later, 40 mg of catalysts was added in the reactor to start

the reaction. The reaction was continuously carried out for 60 min. At a fixed interval, the concentration of phenol and products was analyzed using HPLC and a UV detector. The column used was C-18 with a mobile phase of 30% methanol and 70% ultrapure water. To terminate primary radical species formed during the oxidation process and avoid over-oxidation of phenol, quenching experiments were conducted by the addition of special alcohols (ethanol). Additionally, to evaluate the stability of the catalysts, the sample after one trial was collected through centrifugation, washed by water and ethanol alternatively, and dried for the subsequent cycle test.

3. Results and discussion

Illustration for the synthetic method

Scheme 1 illustrated the synthetic process for this Co-modified HMS nanocomposite. The mechanism of self-assembly was proposed through a metal-assisted templating route ($S^0M^+I^-$). Wherein, the metal cations play an important intermediary role in this templating method by the physical-chemical interaction between surfactant and silicate species. Typically, metal cations (M^+) first coordinated with neutral surfactant of dodecyl amine (DDA, S^0) to generate a metallomicelle which is similar to cationic-like template. The characteristic of metallomicelles is that the surface of micelles is enriched with massive cobalt ions. Then the negatively charged silicate oligomers (I^-) assembled on the surface of metallomicelles by electrostatic interaction. Finally, this nanocomposite with thin-layer-like CoO species on its mesoporous wall would be produced after annealing to remove the template. Taken together, the metallomicelle template is the key factor in determining formation of resulting materials.

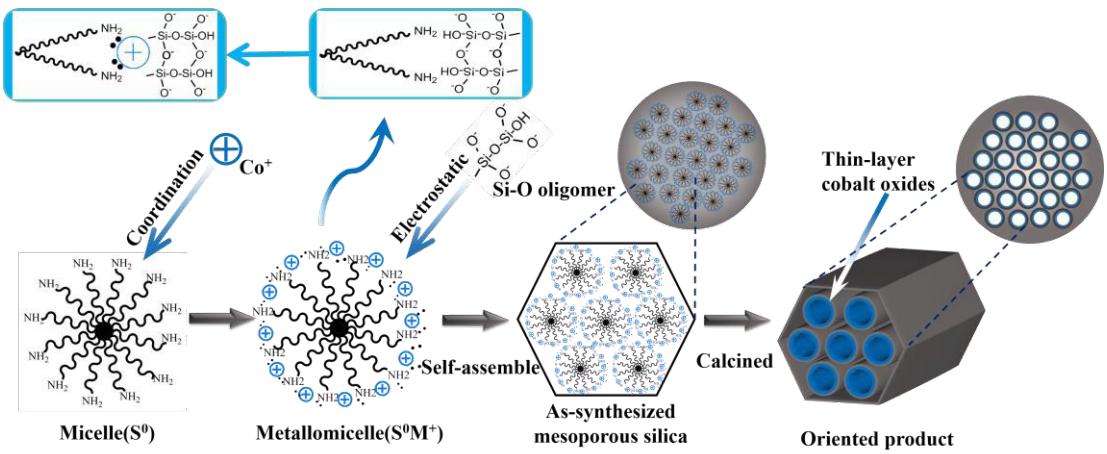

Scheme 1 Metal-assisted templating route ($S^0X^+I^-$) for synthesis of nanospherical HMS-Co

In order to demonstrate the metallization of DDA micelles, corresponding experimental phenomena and results are recorded. Fig. S1 exhibits the UV-vis absorption spectra of DDA micelles, metallomicelles and cobalt chloride solutions. No absorption peak is detected for the spectrum of DDA aqueous solution in the spectra, while the metallomicelles solution from the mixture of DDA and cobalt chloride shows several apparent absorption peaks at 570 nm and 640 nm as compared with that of cobalt chloride solution which are ascribed to transitions n→σ* from ligands (N) to metal ions (Co^{2+}). The finding indicates the coordination of cobalt ions and the amino groups (NH_2-) in DDA. Additionally, the color changing of the metallomicelles solution can be observed before and after mixture of fore-mentioned two solutions though the digital photos of DDA micelles (a), metallomicelles (b) and cobalt chloride (c) aqueous solutions (the insert image of Fig. S1). The colors of single DDA and cobalt chloride aqueous solution are white and red, respectively. In comparison, the mixture of DDA and cobalt chloride appears to be dark green. This observation should be due to the orbital transitions e_{2g}→t_{2g} of metal cobalt ions due to the formation of complexes by the coordination of cobalt ions and the amino groups of DDA. Additionally, it should be

noted that no deposition was observed in the mixture, indicating no formation of cobalt hydroxide (pink) in the process of metallization of micelles.

On the other hand, to our best knowledge, the nitrogen atom in DDA is in the form of secondary amine with lone-pairs of amine. Accordingly, the DDA solution is alkaline with a pH value of 11.4. The pH values of Co^{2+}-DDA solution with altering cobalt ion concentration are summarized in Table S1. An obvious drop in the pH values is detected by increasing the amount of cobalt chloride. Meanwhile, no any deposition from hydrolysis of cobalt ions presents in the solution of mixed micelles, indicating that the drop of pH in this system cannot be ascribed to the hydrolysis of cobalt ions. Therefore, the result should be due to the fact that the metal ions consumed the numbers of lone-pairs in DDA molecules by coordinating with nitrogen atom, thus the pH value of the DDA solutions can drop with an increasing concentration of cobalt. Taken together, these results confirmed the formation of DDA-cobalt complexes by coordination bonds.

Structural properties

The low-angle XRD patterns of pure HMS and series samples of HMS-xCo in the 2θ-range of 1° to 8° are given in Fig. 1a. All samples exhibit a (100) diffraction peak at 2θ=1.5-2.5°, which suggests the presence of mesostructure. With an increasing amount of cobalt ions, the (100) diffraction peak shifts to the low angle from HMS to HMS-3Co indicating the increase of d_{100} interplanar spacing. The finding should be due to the enlargement of DDA micelles by the coordination with cobalt ions. As for HMS-4Co, the (100) diffraction peak shifts to the large angle as compared to HMS-3Co, implying the over-introducing of cobalt ions results in the distortion of DDA micelles. Compared with other samples, the sample of HMS-3Co shows the strongest (100) reflection peak in Fig. 1a. This observation indicates that the cobalt ion concentration should be suitable

for DDA micelle ligands, then the metal cations (M^+) can positively assist the assembly of negatively charged silicate oligomer (I^-) into the ordered mesostructure of HMS-xCo.

The further textural information is obtained by N_2 adsorption-desorption isotherms analysis and their results are shown in Fig. 1b. The corresponding structural parameters of some samples are summarized in Table 2. The typical IV isotherms with an obvious capillary condensation step between 0.2 and 0.4 of P/P_o are clearly observed, indicating the presence of framework mesoporosity in HMS-xCo samples. As the cobalt ion concentration is increased to 0.3 (molar ratio) of Co^{2+}/DDA, the sample HMS-3Co shows the sharpest capillary condensation step and the largest specific surface area (S_{BET}). While at higher concentration of cobalt ion, HMS-4Co shows the dropped structural parameters. This result suggests that a proper amount of cobalt ions can improve the order degree of mesostructure of HMS-xCo via the ($S^0M^+I^-$) route. The higher concentration of cobalt ions would distort the DDA micelles by electrostatic repulsion between metal cations. Whereas, the cobalt cations could not positively work as an intermediate ion (M^+) to promote the assembly between S^0 and I^- at lower concentration. The result is consistent with the XRD observations. Additionally, it should be noted that the wall thickness of Co-modified HMS is increased with cobalt ions coordinated on the micelles. The increase of wall thickness obviously is ascribed to the surface-enriched cobalt oxide species produced during the annealing process.

Interestingly, the absorption volume of sample is closely associated with the loading of cobalt in the samples. When the Co^{2+}/DDA is 0.3, the sample of HMS-3Co exhibits the highest absorption capacity, and the absorption volume is up to 3.19 cm^3/g, which is much higher than the normal mesoporous silica reported.[29, 31] Additionally, the curve of adsorption displays a sudden-upward at high relative pressure, which may indicate the massive presence of bulk void in the sample. This result should be associated with the

size changing of particle by addition of different cobalt amount.

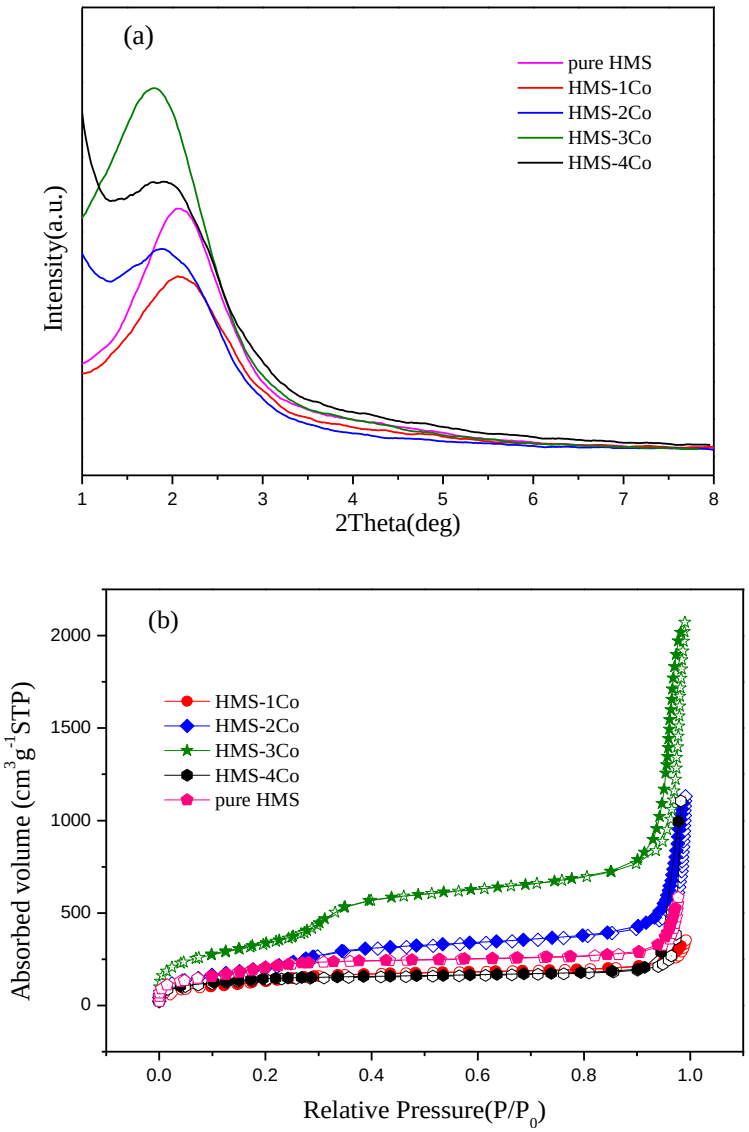

Fig. 1 Low-angle XRD patterns (a) and N_2 adsorption/desorption isotherm (b) of some samples

Table 1 Physical and textural properties of Co-HMS samples.

Samples	Co/Si[a] (%)	S_{BET} ($cm^2 \cdot g^{-1}$)	Pore volume ($cm^3 \cdot g^{-1}$)	d_p[b] (nm)	d-spacing d_{100}[c]	Unit cell parameter [d] a(nm)	Wall thick [e] d_w(nm)
Pure HMS	0	812.9	0.903	2.31	4.239	4.895	2.585
HMS-1Co	2.179	540.2	0.517	2.21	4.194	4.843	2.633
HMS-2Co	4.139	777.6	1.711	2.43	4.640	5.358	2.928
HMS-3Co	6.127	1278.1	3.191	2.62	4.900	5.658	3.038
HMS-4Co	7.033	652.3	1.709	2.13	4.672	5.394	3.264

HMS-3Co(d)	6.314	657.2	0.645	2.24	4.221	4.874	2.63
HMS-3Co(p)	6.182	513.5	0.421	1.92	4.964	5.732	3.81

[a] Calculated from ICP data.

[b] Pore sizes obtained from BJH analysis of desorption data.

[c] $d_{100}=\lambda/2\sin\theta$.

[d] $a_0=2d_{100}/\sqrt{3}$.

[e] $d_w=a_0-d_p$.

The representative SEM images of samples of pure HMS (a), HMS-1Co (b), HMS-2Co (c), HMS-3Co (d) and HMS-4Co (e) are shown in Fig. 2. All of the SEM images of the given samples exhibit a round-like morphology. The pure HMS shows typical spherical characteristic even with large and nonuniform sizes of particle. In addition, it is worth noting that by comparison of sample containing different cobalt loading, obviously, the samples particles of HMS-3Co possesses the minimum particle size of ca. 150-200 nm. The size of particle is decreased with cobalt ions in the samples from HMS-0Co to -3Co, accordingly, the aggregation voids from the stacking of particles became larger, which is in good agreement with the above-mentioned N_2 adsorption analysis. It suggests that loading of cobalt may influence the particles size of samples. The formation of spherical HMS-Co particles should be based on a surface-energy-dominated process. The formation of metallomicelles in the assemble process may lead to increasing repulsion among the micelles and make the nucleated particles assembled from the metallomicelles and silicate oligomers hard to aggregate into a larger sphere.

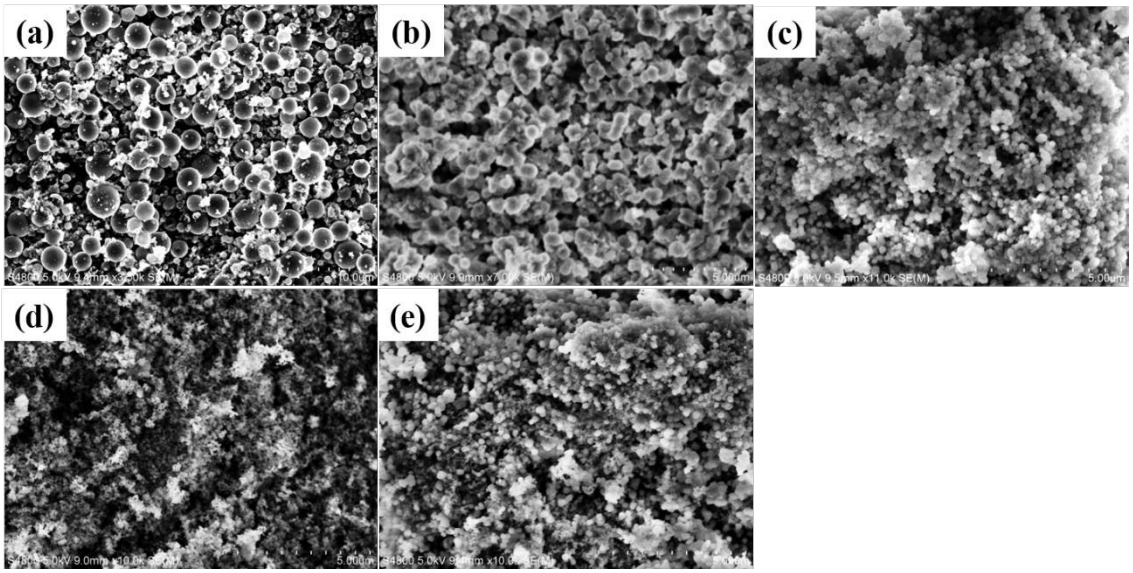

Fig. 2 Representative SEM images of samples of pure HMS (a), HMS-1Co (b), HMS-2Co (c), HMS-3Co (d) and HMS-4Co (e).

The states of cobalt species

The high-angle XRD patterns of series samples of HMS-xCo (direct templating method), Co-doping sample of HMS-3Co (d) and post-impregnated sample of HMS-3Co (p) are displayed in Fig. 3. As for series samples of HMS-xCo from templating method, no obvious diffraction peak of cobalt compounds is detected in their curves. The absence of diffraction peaks of cobalt species suggests no formation of crystalline CoO during the annealing process of samples. This result also manifests the high-dispersion of CoO species on the mesoporous silica. This may be due to that the strong interaction of metal ions and silicate wall stabilize the Co atoms and prohibit their immigration and aggregation in the annealing process. Meanwhile, the Co-doping sample of HMS-3Co (b) shows a similar result, which indicates that the cobalt should be incorporated in the framework of mesoporous silica. Additionally, it should be noted that several crystal diffraction peaks located at 31.25°, 36.8°, 44.8°, 59.35° and 65.2° are observed in the curve of sample of HMS-3Co (p) and indexed to [220], [311], [400],

[511] and [440] diffraction peaks of cobalt oxide (Co_3O_4) crystals. This phenomenon indicates the formation of aggregated cobalt oxide crystals for the sample of HMS-3Co (p) prepared by the post-impregnation.

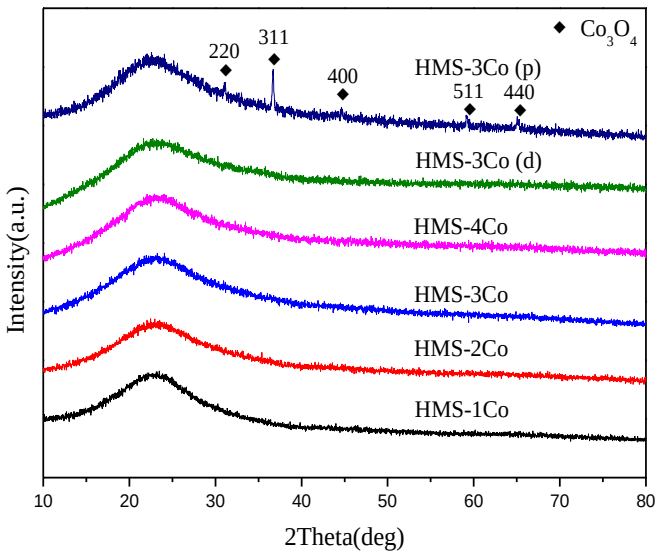

Fig. 3 High-angle XRD patterns of series samples of HMS-xCo, HMS-3Co (d) and HMS-3Co (p)

In order to have a deep insight into the distribution of cobalt species and the morphology of the samples, the typical sample of HMS-3Co was further characterized by TEM, STEM technique and elemental mapping analysis. As is shown in Fig. 4a, 4b, 4c, the TEM images of sample of HMS-3Co show a spherical morphology of particles, additionally, the present wormhole-like pore and sponge-like frame structure is in accordance with reported literature.[32] The cobalt oxide nanocrystals are invisible in TEM images, indicating the high-dispersion of cobalt species in HMS. Furthermore, in Fig. 4d, STEM-HAADF image shows no obvious light spot in sample, which indicated no formation of CoO nanocrystals. The CoO species should be existed with the form of amorphous status. The elemental mapping analysis exhibits that the HMS material from the templating method contained elements of Si, O, and Co. Also, it is clear that the

cobalt elements are uniformly dispersed on the spherical HMS, which could confirm the high dispersion of Co species. On the basis of these observations, it indicates that the one-pot $S^0M^+I^-$ route for HMS-Co can contribute to the uniform dispersion of cobalt species.

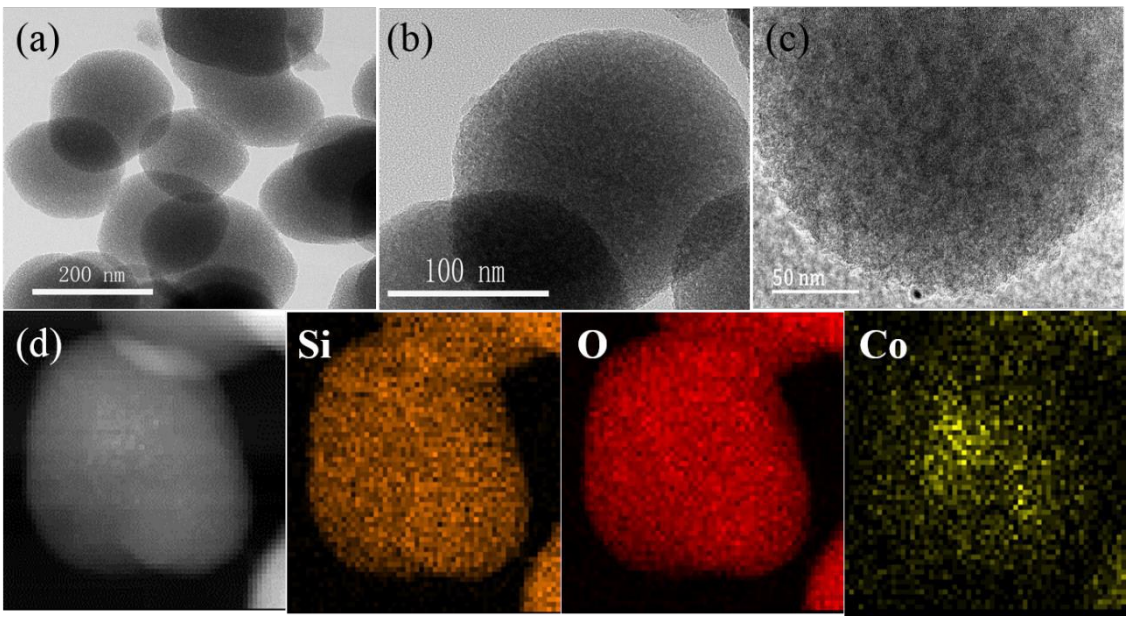

Fig. 4 Representative TEM images (a), (b), (c) and Dark-field STEM images (d) and elemental mapping analysis of sample HMS-3Co.

FT-IR spectra of the calcined series samples of HMS-xCo and uncalcined samples of pure HMS-DDA and HMS-3Co-DDA are shown in Fig. 5. As we observed, the sample of pure HMS-DDA exhibits a typical as-synthesized HMS material characteristic curve, additionally, the peak at ca. 2932 cm^{-1} is obviously attributed to the absorbed band of the surfactant.[33] Note that an additional peak at 718 cm^{-1} is observed for the sample of HMS-3Co-DDA, which may be ascribed to Co-N band due to the formation of Co^{2+}-DDA complexes. Another surface information presenting in these spectra can manifest the distribution of cobalt oxide species on the mesopore. Typically, the absorption peak at 964 cm^{-1} corresponding to the stretching vibration of Si-O-H surface groups[34] can be

observed. However, it is worth noting that the absorption peaks assigned to Si-O-H surface groups are weakened gradually with increasing content of cobalt. The reduction of Si-O-H surface groups should be due to the increasing coverage of cobalt oxide species on their surface.[35]

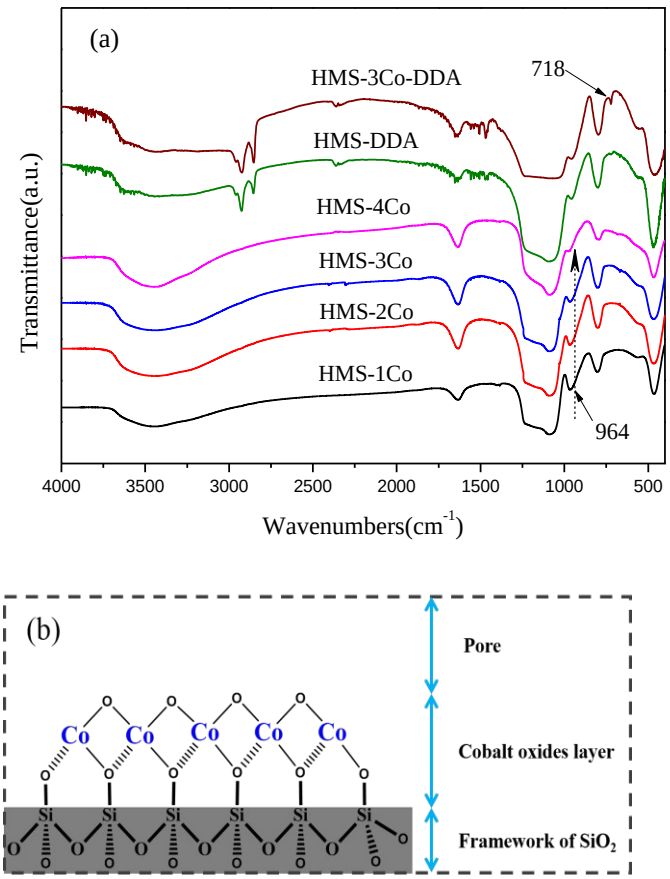

Fig. 5 FT-IR spectra (a) of series samples of HMS-xCo and feasible surface structure of Co-modified pore wall in the sample synthesized by templating method (b).

The UV-vis spectroscopy is considered as an effective technique for studying the local coordination environment and electronic state of isolated transition metal ions as well as aggregated metal oxides. Some authors reported that the features of the spectra are closely related to the degree of crystallinity of the supported cobalt oxide particles.[36, 37] The UV-vis spectra of series samples of HMS-xCo are shown in Fig. 6. All HMS-xCo samples exhibit three distinct absorption bands in the range of 450-700 nm, which

are centred at 525, 588 and 644 nm, respectively and ascribed to the ligand field d–d electron transitions, $^4A_2(F) \rightarrow {}^4T_2(F)$, $^4A_2(F) \rightarrow {}^4T_1(F)$ and $^4A_2(F) \rightarrow {}^4T_1(P)$, characteristic of Co^{2+} ions in tetrahedral coordination and the blue colour of the samples further supports this assignment.[38] According to ref.[39, 40] they could be included in highly dispersed amorphous cobalt oxide species strongly interacting with the surface of silica support.

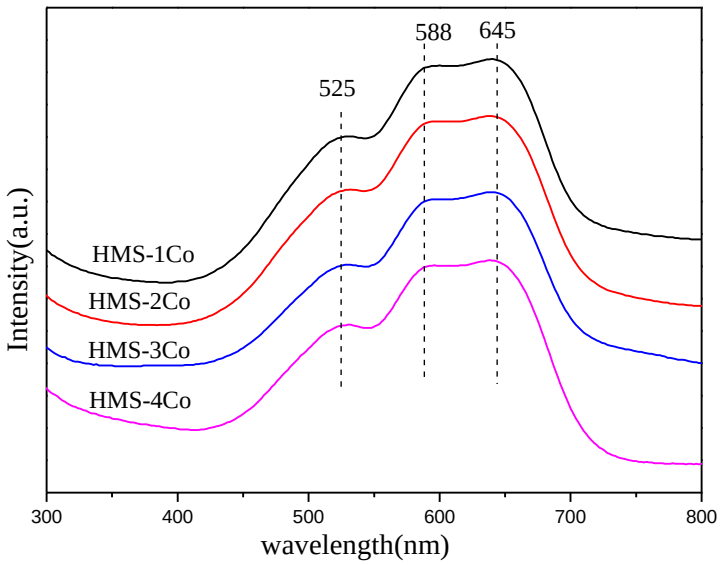

Fig. 6 DRUV-vis spectra of series samples of HMS-xCo

In order to accurately investigate the elemental chemical state of the samples, high-resolution XPS spectra for Co 2p of uncalcined HMS-3Co (a) and calcined HMS-3Co (b), N 1s of uncalcined HMS-3Co (c) and pure HMS (d) are recorded in Fig. 7. Primarily, the binding energy value of Co 2p transition splits located at 780.9 and 797 eV for the $2p_{3/2}$ and $2p_{1/2}$, along with two shake-up satellite peaks at ca. 787 and 803 eV are observed respectively for the uncalcined HMS-3Co. As for the calcined HMS-3Co, four peaks of Co $2p_{3/2}$, Co $2p_{1/2}$ and their two shake-up satellites corresponding to binding energy at 781.8, 797.9, 789 and 803.6 eV present in the its curve. The orbital

splitting between $2p_{1/2}$ and $2p_{3/2}$ peaks is ca. 16.1 eV for the two sample, which is in accordance with that of Co^{2+} (16.0 eV) rather than Co^{3+} compounds (15.0 eV).[38, 41] It clearly indicates that the cobalt species present mainly in Co(II) oxidation state before and after calcination, which is in good agreement with the UV-vis result. However, it should be noted that the binding energy position of Co 2p of calcined HMS-3Co exhibits an obvious shift to high value as compared to uncalcined HMS-3Co. This phenomenon manifests that the Co atoms do not stably existed in the framework of mesoporous silica and the chemical environment of Co atoms has be altered during the annealing process. Therefore, the result as strong evidence supports that the Co species must present in the surface of mesoporous silica.

Additionally, as compared with the binding energy of pure CoO (780 eV)[42] and Co species (782.2 eV) incorporated in silicate framework,[43] the binding energy of cobalt oxide in calcined HMS-xCo have a different value of 781.8 eV between the above two values, indicating that the cobalt oxide species should be interacted with the silicate wall and present on its surface. Additionally, the presence of the shake-up satellite is indicative of the presence of Co^{2+} species and also can be taken as evidence of a strong interaction between the Co^{2+} species and the Si-O bond on the surface of HMS.[43-45] These findings accorded with the UV-vis and FT-IR results.

On another hand, the N 1s spectra of uncalcined pure HMS and HMS-3Co display two obviously different results for the binding energy of N atoms in the samples. The N 1s spectrum of the uncalcined pure HMS shows two peaks corresponding to binding energy at 399.65 and 401.3 eV. Wherein, the peak with binding energy at 399.65 eV is attributed to the free amino groups of DDA,[46] and its shoulder peak at 401.3 eV should be ascribed to amino groups interacted with silicate wall by hydrogen-bonding. Whereas, the N 1s spectrum of the uncalcined HMS-3Co shows two peaks located at

399.65 and 401.65 eV. The peak located at 399.65 eV is in accordance with that of aforementioned pure HMS, however, its shoulder peak is obviously different from that ascribed to hydrogen-bonding. An obvious shift (0.35 eV) to high value and enhanced intensity are observed in the curve. The peak should be associated with the amino groups coordinated with Co ions presenting on the micelles, where the electron-enriched nitrogen atoms shared electrons with Co ions and thus electron densities of nitrogen atoms are reduced.[47]

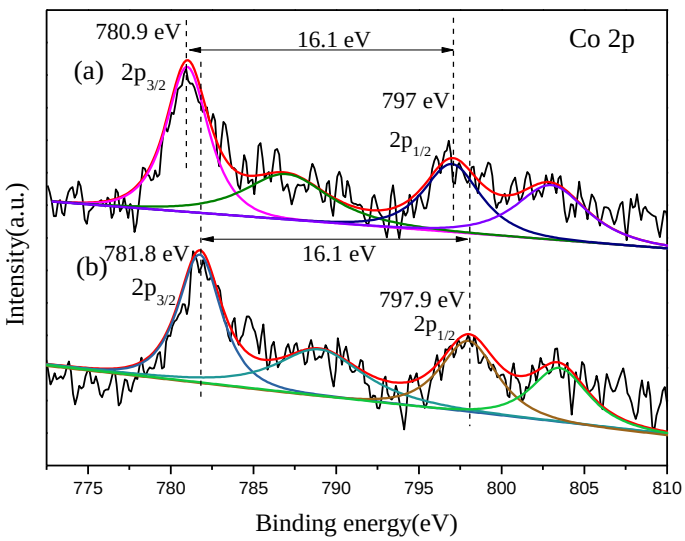

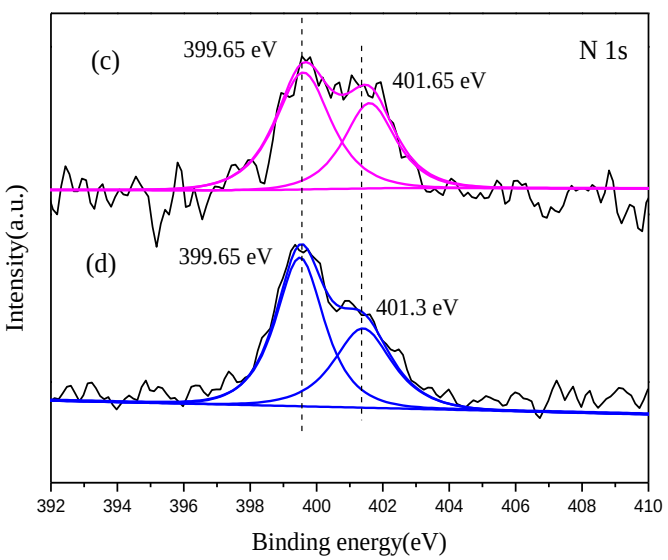

Fig. 7 High-resolution XPS spectra: Co 2p spectra of uncalcined sample of HMS-3Co (a) and calcined sample of HMS-3Co (b), N 1s spectra of uncalcined sample of HMS-3Co (c) and pure HMS (d)

Catalytic results

The catalytic performance of series samples of HMS-xCo was evaluated by direct oxidation of phenol in the presence of oxone, and the termination of radical in the end of reaction was carried out using ethanol (EtOH) as quenching agents for avoiding the over-oxidation of phenol. Previous researches have revealed that EtOH (with a-hydrogen) as an efficient quenching agent can rapidly react with both hydroxyl and sulfate radicals to terminate the reaction, with the reaction rate constants of 1.2×10^9–2.8×10^9 and 1.2×10^9–2.8×10^9 $M^{-1}s^{-1}$, respectively.[48, 49] In addition, in order to investigate the specificity of the nanospherical HMS catalyst synthesized by the templating method, corresponding comparative experiments for the oxidation of phenol using only PMS, pure HMS, homogeneous cobalt ions, Co-doping HMS and post-impregnation Co-modified HMS were carried out.

Herein, the corresponding catalytic results are displayed in Fig. 8(a, b, c, d and e) and the further detail catalytic data are summarized in Table 2. The initial reactant and final products were confirmed by HPLC and UV-vis. In Fig. 8a, two ultraviolet absorption peak located at 270 nm and 246 nm could be observed which are ascribed to phenol and p-benzoquinone, respectively. Moreover, the catalytic dynamic results were also monitored by a UV detector, typically, as we can see in Fig. 8b, the UV absorption peak shifts from 270 nm to 246 nm because of the disappearing of phenol and formation of p-benzoquinone. The absorption intensity at 270 nm become weaker and weaker along with the increase of reaction time, meanwhile, an absorption peak around 246 nm

appears and become enhanced due to the formation of p-benzoquinone. It is worth noting that no other obvious UV absorption peak is detected even in the end of reaction, which indicates other products should be few as compared to p-benzoquinone. As for the reaction with only PMS without a solid catalyst, decaying of phenol is negligible during 60 min, indicating that the PMS itself could not be activated for oxidizing phenol under the same condition. The phenol concentration shows no evident change in the presence of pure HMS, which suggests that the consumption of phenol by adsorption process could be ignored. With regard to the reaction using homogeneous $CoCl_2$ solution, the reaction shows a quicker reaction rate for the phenol decay, however, it should be noted that the p-benzoquinone generating from the oxidation of phenol shows a poor selectivity. This is attributed to the quick consumption of p-benzoquinone to degradation due to the presence of much more sulfate radicals stimulated from homogeneous Co^{2+}. Meanwhile, another two comparative samples both of HMS-3Co (d) and HMS-3Co (p) display inferior catalytic result as compared to that of HMS-3Co synthesized by templating method. This results should be due to the synergy of high structural properties and highly-dispersed catalytic active sites in the oxidation of phenol to p-benzoquinone. Wherein, the high-dispersion of CoO active sites mainly contributes to the high catalytic results, which can be indicated by the comparison of structural properties, metal loading and catalytic performance of samples. Just as observed in Table 1, the sample of HMS-1Co exhibits similar structural properties in comparison to the HMS-3Co (p). However, the sample HMS-1Co shows the same catalytic conversion as compared to HMS-3Co (p), even the HMS-3Co (p) possesses the much higher CoO loading. This is obviously due to the high contribution of highly-dispersed CoO enriched on the pore wall. Therefore, we think that the high-dispersion of CoO is dominated for receiving high catalytic conversion in the catalytic process. In

addition, the high textural properties are also the positive factors for contributing to high catalytic activity. On basis of the result, a reasonable explanation could be proposed that the catalytic active sites supported on the aforementioned two Co-modified samples is insufficient as compared to HMS-3Co even they possess a similar loading of cobalt. Associating with aforementioned characterization analysis, the post-impregnation Co-modified HMS possesses aggregated bulk cobalt oxide, therefore, the exposed active sites are lacked. Besides, the active phase presenting in the post-impregnation sample exists with the form of Co_3O_4. The present Co(II) is lower than CoO phase in the directly synthesized HMS-3Co. As for the Co-doping HMS-3Co (d), a large amount of cobalt atoms should be incorporated in the framework of the sample of HMS-3Co (d), therefore, the Co species on the surface are lower.

To have a better understanding of the reaction kinetics of the phenol oxidation catalyzed by the heterogeneous hybrid Co-modified HMS catalysts, a general pseudo-first-order kinetics for phenol decay could be assumed: $\ln(C_0/C)=kt$, where C_0/C represents the normalized phenol concentration and k is the apparent reaction rate constant.[47] The linear relationship using series samples of HMS-xCo and two comparative Co-modified HMS-3Co (d), (p) between $\ln(C_0/C)$ and reaction time of the oxidation reaction is demonstrated in Fig. 8d, where C and C_0 are the concentration of phenol at different time (interval time is 2 min) and initial time, which can be measured from the relative intensity of the absorbance C and C_0, respectively. By the comparison of calculated *k* constant of different samples, obviously, the sample of HMS-3Co shows the highest value, indicating its most efficiency in this reaction. The *k* constant is enhanced with increasing cobalt loading in the series sample HMS-1Co, -2Co, -3Co. However, the sample of HMS-4Co shows a lower *k* value as compared with HMS-3Co, which is in accordance with aforementioned characterized results. In addition, the

stability test of catalyst was carried out where HMS-3Co as optimal sample is selected, and the result is shown in the Fig. 8e. With six recycling tests, the sample of HMS-3Co exhibits a sustained catalytic activity for the oxidation of phenol. This result demonstrates the high stability of sample synthesized by templating method. In addition, in order to investigate the status of Co atoms in the used catalyst, the HMS-3Co used for three times was tested using DRUV-vis spectra (Fig. S5). The DRUV-vis spectra of HMS-3Co used for three times is similar to that of HMS-3Co and no Co(III) is not detected. The result reveals the recovered catalyst possesses the Co(II) active sites after undergoing several catalytic recycles. The high stability should be attributed to the strong interaction between CoO species and silicate wall (Fig. 5b).

Previous studies of supported cobalt-based catalyst have reported for highly-efficient degradation of phenol, instead, the series samples of HMS-xCo synthesized via the templating method exhibits special catalytic activities for the synthesis of p-benzoquinone by oxidation of phenol in the presence of peroxymononsulfate. Additionally, the detection results from HPLC and UV-vis do not show any other product except for catechol, hydroquinone and p-benzoquinone. This is an obviously different result as compared to that of the reported paper. The special catalytic results are attributed to relatively mild catalytic oxidation capacity for the heterogeneous CoO species supported on the HMS as compared to the homogeneous Co ions. Besides, the timely termination of radicals by the addition of EtOH also leads to no excessive oxidation of aforementioned products in the oxidation process of phenol. This result would give us more profiles about oxidation of phenol to synthesize the expected p-benzoquinone by the Fenton-like type catalyst rather than excessive oxidation of phenol to degrade.

According to the ref.[50, 51] the radical generation and oxidation of phenol processes can be described as follows and the entire oxidation process was further clear displayed in Scheme 2.

$Co(II) + HSO_5^- \rightarrow Co(III) + SO_4^{\bullet -} + {\bullet}OH$ (1)

$2HSO_5^- + 2{\bullet}OH \rightarrow 2SO_4^{\bullet -} + 2H_2O + O_2$ (2)

$Co(III) + HSO_5^- \rightarrow Co(II) + SO_5^{\bullet -} + H^+$ (3)

$2SO_5^{\bullet -} + 2OH^- \rightarrow 2{\bullet}OH + 2SO_4^{2-} + O_2$ (4)

${\bullet}OH + SO_4^{\bullet -} + C_6H_5OH \rightarrow C_6H_5OH{-}SO_4^{\bullet -} \rightarrow C_6H_5OH^{\bullet +} + SO_4^{2-} \rightarrow$ catechol, hydroquinone and p-benzoquinone$\rightarrow$ termination (5)

Primarily, Co-modified HMS nanosphere activates PMS to generate hydroxyl radicals and sulfate radicals (Eq. (1)). Then some of the produced hydroxyl radicals would further stimulate PMS to produce more sulfate radicals (Eq. (2)). However, the sulfate radicals are depleted in a short time by rapid reaction with phenol. During the phenol oxidation by sulfate radicals, hydroxyl radicals also participated, though at an inferior reaction rate (Eq. (5)). After the consumption of sulfate radicals, hydroxyl radicals become the only reactive species reacting with phenol. Meanwhile, the recovery reactions for the nanospherical Co-modified HMS materials results in the production of original state of the catalyst as well as the further generation of hydroxyl radicals (Eq. (3-4)). At the same time, competitive reactions may also happen which might negatively affect the generation of reactive species (Eq. (5)). On the basis of the comprehensive thoughts, it is suggested that the hydroxyl radicals generated by Co-modified HMS initially determines the order of phenol oxidation.

Table 2 the direct oxidation of phenol to p-benzoquinone in the presence of PMS using series Co-modified HMS.

	Selectivity (%)	Apparent rate

Samples	Co/Si [a]	Conversion (%)	BQ [b]	HQ [c]	CAQ [d]	others	constant, k/min^{-1}
Pure HMS	-	0	-	-	-	-	-
$CoCl_2$	-	75	42	16	18	24	0.0378
HMS-3Co(p)	6.182	42	61	9	24	6	0.0091
HMS-3Co(d)	6.314	54	67	6	17	10	0.0126
HMS-1Co	2.179	42	73	7	16	4	0.0092
HMS-2Co	4.139	57	78	6	13	3	0.0179
HMS-3Co	6.127	82	79	5	14	2	0.0287
HMS-4Co	7.033	67	75	8	10	7	0.0171

[a] the data calculated from the ICP results.

[b] BQ represents p-benzoquinone.

[c] HQ represents hydroquinone.

[d] CAQ represents catechol.

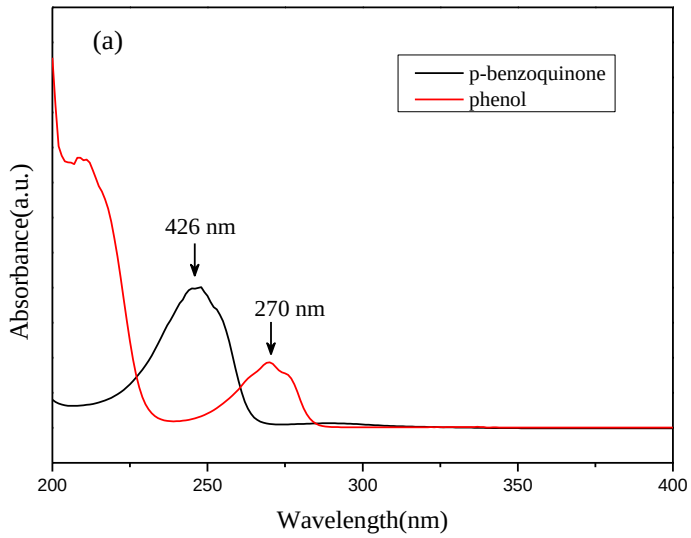

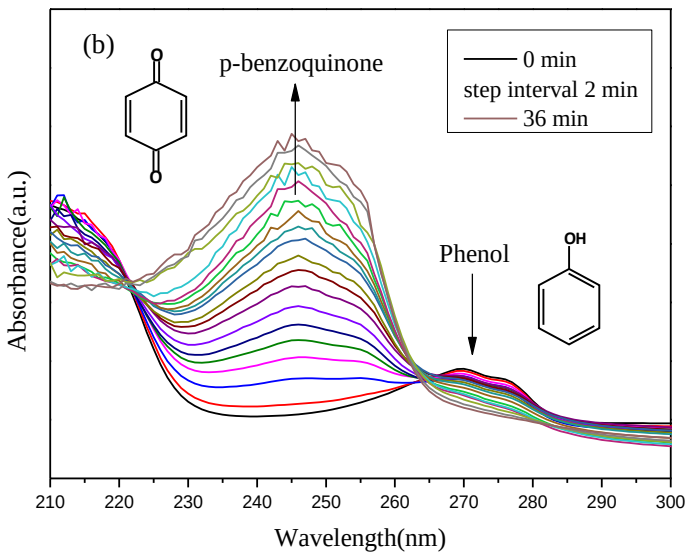

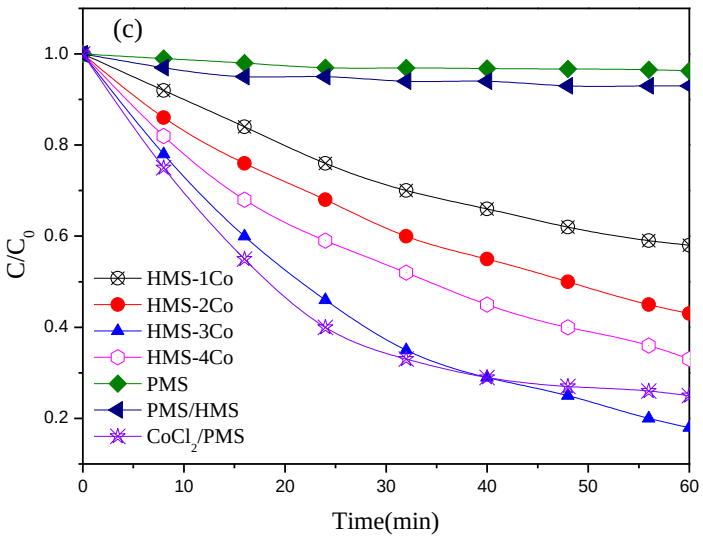

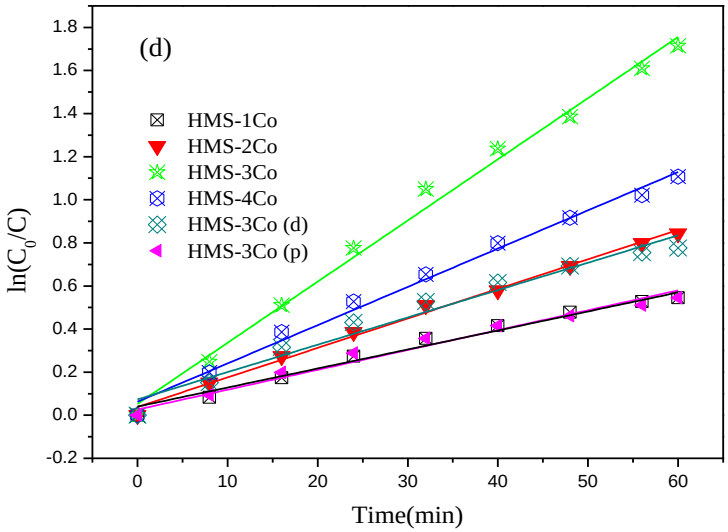

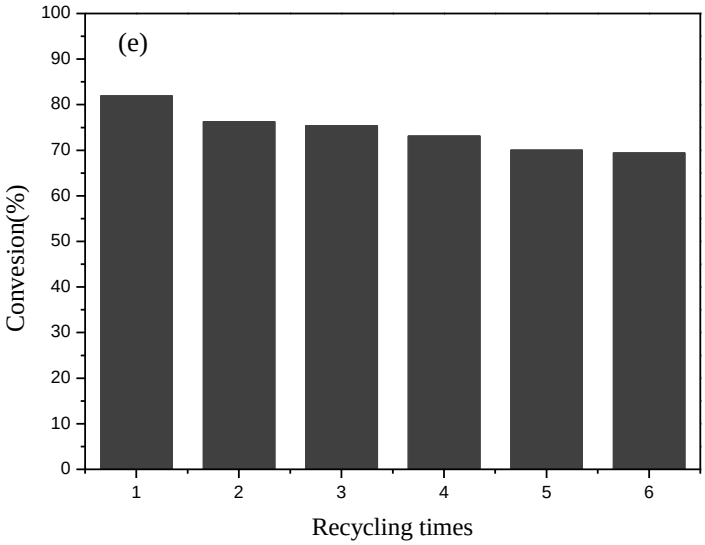

Fig. 8 UV-vis absorption spectra of phenol and p-benzoquinone after adding PMS (a); successive oxidation of phenol using HMS-3Co as catalyst (b); C/C_0 versus reaction time for the oxidation of phenol at 270 nm using only PMS, pure HMS/PMS, $CoCl_2$/PMS and series samples of HMS-xCo as catalysts (c); $\ln(C_0/C)$ versus reaction time for the oxidation of phenol using series samples of HMS-xCo, HMS-3Co (d) and HMS-3Co (p) as catalyst (d). The reusability of HMS-3Co (a) as a catalyst for the oxidation of phenol (e).

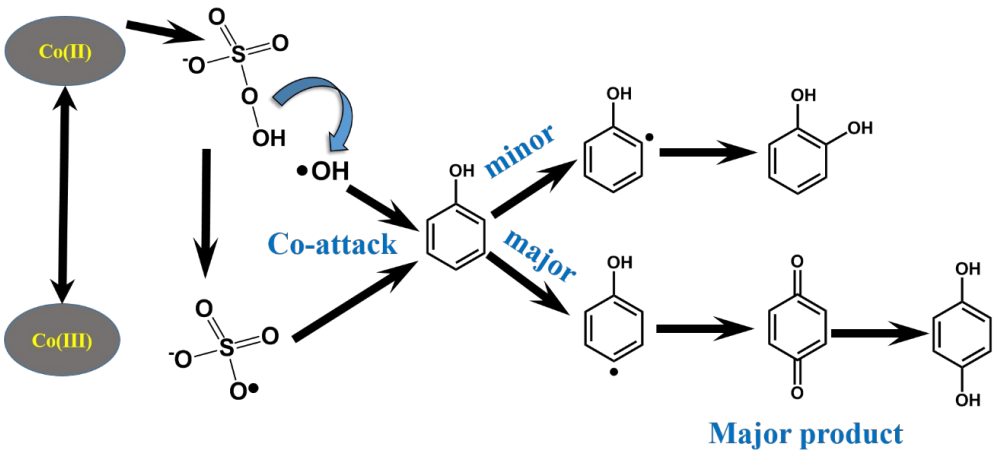

Scheme 2 Assumed mechanism for PMS activation by HMS-Co for phenol oxidation.

4. Conclusions

In conclusion, we developed a novel metal-assisted templating route and successfully prepared nanospherical HMS catalyst possessing highly-dispersed and enriched CoO surface active species and improved structural properties (large surface and pore volume). In addition, surface active sites on the mesochannels can be adjusted by controlling metallization of micelles. Experimental data indicate that metal-assisted templating route facilitates assembly of micelles and silicates and increase numbers of mesopore in the mesocomposites significantly. The obtained nanospherical Co-modified HMS exhibit superior catalytic activities in the oxidation of phenol to p-benzoquinone

by sulfate radicals stimulated from peroxymonosulfate. The mesocomposites' surface covered with 2-dimentional metal oxides would be expected to obtain special properties, not only was limited in catalysis.

Acknowledgements

The authors acknowledge the financial support of the National Natural Science Foundations of China (21276125, 20876077 and 21476108)

Notes and references

1. R. J. Kalbasi, A. R. Massah, F. Zamani, A. D. Bain and B. Berno, *J. Porous Mater.*, 2011, **18**, 475-482.
2. B. Han, H. Wang, Y. Kong and J. Wang, *Mater. Lett.*, 2013, **100**, 159-162.
3. S. Rahman, C. Santra, R. Kumar, J. Bahadur, A. Sultana, R. Schweins, D. Sen, S. Maity, S. Mazumdar and B. Chowdhury, *Appl. Catal. A-Gen.*, 2014, **482**, 61-68.
4. C. Guo, Y. Wu and J. Zhan, *React. Kinet. Mech. Catal.*, 2013, **109**, 497-508.
5. G. P. Anipsitakis, E. Stathatos and D. D. Dionysiou, *J. Phys. Chem. B*, 2005, **109**, 13052-13055.
6. S. Muhammad, E. Saputra, H. Sun, J. d. C. Izidoro, D. A. Fungaro, H. M. Ang, M. O. Tade and S. Wang, *Rsc Adv.*, 2012, **2**, 5645-5650.
7. P. Shukla, H. Sun, S. Wang, H. M. Ang and M. O. Tade, *Catal. Today*, 2011, **175**, 380-385.
8. P. Shukla, S. Wang, K. Singh, H. M. Ang and M. O. Tade, *Appl. Catal. B-Environ.*, 2010, **99**, 163-169.
9. P. R. Shukla, S. Wang, H. Sun, H. M. Ang and M. Tade, *Appl. Catal. B-Environ.*, 2010, **100**, 529-534.
10. J. S. Beck, J. C. Vartuli, W. J. Roth, M. E. Leonowicz, C. T. Kresge, K. D. Schmitt, C. T. W. Chu, D. H. Olson, E. W. Sheppard, S. B. McCullen, J. B. Higgins and J. L. Schlenker, *J. Am. Chem. Soc.*, 1992, **114**, 10834-10843.
11. A. Corma, *Chem. Rev.*, 1997, **97**, 2373-2419.
12. D. Y. Zhao, J. L. Feng, Q. S. Huo, N. Melosh, G. H. Fredrickson, B. F. Chmelka and G. D. Stucky, *Science*, 1998, **279**, 548-552.
13. M. Boero, M. Parrinello, H. Weiss and S. Huffer, *J.Phys. Chem. A*, 2001, **105**, 5096-5105.
14. P. A. Nikulshin, D. I. Ishutenko, A. A. Mozhaev, K. I. Maslakov and A. A. Pimerzin, *J. Catal.*, 2014, **312**, 152-169.
15. J. Hou, Y. Li, M. Mao, L. Ren and X. Zhao, *Acs Appl. Mater. Interf.*, 2014, **6**, 14981-14987.
16. Y. Wu, X. Liu, X. Huang, S. Xing, Z. Ma and L. Feng, *Mater. Lett.*, 2015, **139**, 157-160.
17. J. Qi, J. Chen, G. Li, S. Li, Y. Gao and Z. Tang, *Energ. Environ. Sci.*, 2012, **5**, 8937-8941.
18. J. Qi, K. Zhao, G. Li, Y. Gao, H. Zhao, R. Yu and Z. Tang, *Nanoscale*, 2014, **6**, 4072-4077.
19. G. Li and Z. Tang, *Nanoscale*, 2014, **6**, 3995-4011.
20. K. Zhao, J. Qi, S. Zhao, H. Tang, H. Yin, L. Zong, L. Chang, Y. Gao, R. Yu and Z. Tang, *Chin. J. Catal.*, 2015, **36**, 261-267.
21. K. Zhao, J. Qi, H. Yin, Z. Wang, S. Zhao, X. Ma, J. Wan, L. Chang, Y. Gao, R. Yu and Z. Tang, *J. Mater. Chem. A*, 2015, **3**, 20465-20470.
22. J. Chen, D. Wang, J. Qi, G. Li, F. Zheng, S. Li, H. Zhao and Z. Tang, *Small*, 2015, **11**, 420-425.
23. Q. Zhang, C. Chen, M. Wang, J. Cai, J. Xu and C. Xia, *Nanoscale Res. Lett.*, 2011, **6,** 586-593.
24. N. Zhao, H. Gao, H. Wang, H. He, Y. Chen and Y. Kong, *J. Nanosci. Nanotech.*, 2014, **14**, 7300-7306.
25. H. Wang, W. Qian, J. Chen, Y. Wu, X. Xu, J. Wang and Y. Kong, *Rsc Adv.*, 2014, **4**, 50832-50839.
26. W. H. Zhang, M. Froba, J. L. Wang, P. T. Tanev, J. Wong and T. J. Pinnavaia, *J. Am. Chem. Soc.*, 1996, **118**, 9164-9171.
27. S. Che, A. E. Garcia-Bennett, T. Yokoi, K. Sakamoto, H. Kunieda, O. Terasaki and T. Tatsumi, *Nat. Mater.*, 2003, **2**, 801-805.
28. C. Y. Chen, S. L. Burkett, H. X. Li and M. E. Davis, *Micropor. Mater.*, 1993, **2**, 27-34.
29. P. T. Tanev and T. J. Pinnavaia, *Chem. Mater.*, 1996, **8**, 2068-2079.
30. J. Qin, B. Li, W. Zhang, W. Lv, C. Han and J. Liu, *Micropor. Mesopor. Mater.*, 2015, **208**, 181-187.
31. L. Mercier and T. J. Pinnavaia, *Chem. Mater.*, 2000, **12**, 188-196.
32. W. J. Wang, Y. W. Chen and M. D. Chou, *J. Porous Mater.*, 2004, **11**, 71-78.
33. Z. H. Fu, J. H. Chen, Y. D. Chen, Y. H. Xiang, L. X. Zhang and D. L. Yin, *Acta Phys. Chim. Sin.*, 2000, **16**, 410-415.
34. E. Caponetti, A. Minoja, M. L. Saladino and A. Spinella, *Micropor. Mesopor. Mater.*, 2008, **113**, 490-498.

35. F. Yang, S. Gao, C. Xiong, S. Long, X. Li, T. Xi and Y. Kong, *Rsc Adv.*, 2015, **5**, 72099-72106.
36. K. Kojima, H. Taguchi and J. Matsuda, *J. Phys. Chem.*, 1991, **95**, 7595-7598.
37. I. N. Martyanov, S. Uma, S. Rodrigues and K. J. Klabunde, *Langmuir*, 2005, **21**, 2273-2280.
38. S. S. Bhoware, S. Shylesh, K. R. Kamble and A. P. Singh, *J. Mol. Catal. A-Chem.*, 2006, **255**, 123-130.
39. T. Tsoncheva, J. Rosenholm, M. Linden, F. Kleitz, M. Tiemann, L. Ivanova, M. Dimitrov, D. Paneva, I. Mitov and C. Minchev, *Micropor. Mesopor. Mater.*, 2008, **112**, 327-337.
40. T. Tsoncheva, L. Ivanova, J. Rosenholm and M. Linden, *Appl. Catal. B-Environ.*, 2009, **89**, 365-374.
41. J. Taghavimoghaddam, G. P. Knowles and A. L. Chaffee, *J. Mol. Catal. A-Chem.*, 2012, **358**, 79-88.
42. H. Yang, J. Ouyang and A. Tang, *J. Phys. Chem. B*, 2007, **111**, 8006-8013.
43. Y. Dong, X. Zhan, X. Niu, J. Li, F. Yuan, Y. Zhu and H. Fu, *Micropor. Mesopor. Mater.*, 2014, **185**, 97-106.
44. A. Martinez, C. Lopez, F. Marquez and I. Diaz, *J. Catal.*, 2003, **220**, 486-499.
45. P. A. Robles-Dutenhefner, K. A. da Silva Rocha, E. M. B. Sousa and E. V. Gusevskaya, *J. Catal.*, 2009, **265**, 72-79.
46. H. Yu, Y. Zhu, H. Yang, K. Nakanishi, K. Kanamori and X. Guo, *Dalton T.*, 2014, **43**, 12648-12656.
47. Y.-P. Zhu, T.-Z. Ren and Z.-Y. Yuan, *Rsc Adv.*, 2015, **5**, 7628-7636.
48. G. V. Buxton, C. L. Greenstock, W. P. Helman and A. B. Ross, *J. Phys. Chem.*, 1988, **17**, 513-886.
49. P. Neta, R. E. Huie and A. B. Ross, *J. Phys. Chem.*, 1988, **17**, 1027-1284.
50. Y. Wang, S. Indrawirawan, X. Duan, H. Sun, H. M. Ang, M. O. Tade and S. Wang, *Chem. Eng. J.*, 2015, **266**, 12-20.
51. T. Olmez-Hanci and I. Arslan-Alaton, *Chem. Eng. J.*, 2013, **224**, 10-16.